Integral Solution of Unsteady Full-Potential Equation for a Transonic Pitching Airfoil

Osama A. Kandil* and Hong Hu†
Old Dominion University, Norfolk, Virginia

The unsteady full-potential equation formulation in a moving frame of reference has been developed and used to solve unsteady transonic flow problems. An unsteady integral-equation shock-capturing (IE-SC) scheme has been developed. The resulting unsteady IE-SC scheme is applied to a NACA 0012 airfoil undergoing a pitching oscillation. The numerical results are compared with those of an implicit, approximately factored, finite-volume Euler scheme. The present scheme is efficient in terms of the number of iterations as compared to the other existing schemes, which use finite-difference or finite-volume methods.

Introduction

ONE of the main difficulties facing the aircraft designer is predicting the aerodynamic loads at transonic speeds. The mixed nature and the nonlinearity of the flow equations are at the root of the difficulty. For unsteady flows under certain conditions, aircraft structures like wings and tail surfaces may experience vibrations of an unstable nature. This aeroelastic phenomenon is called "flutter." The accuracy of the flutter prediction depends mainly on the knowledge of unsteady aerodynamic forces. For unsteady transonic flows at low to moderate reduced frequencies, the governing equation of the flow cannot be linearized in contrast with the unsteady subsonic or supersonic flows. This means that the unsteady transonic flowfield cannot be treated independently of the steady flowfield. This makes the unsteady transonic flow problems considerably complicated.

The computation of unsteady transonic flows using finite-difference and finite-volume methods started in 1975. Using different levels of mathematical approximations, inviscid unsteady computational schemes have been developed based on the low-frequency, transonic, small-disturbance (TSD) equation,[1-3] the complete TSD equation,[4-7] the full-potential equation,[8-10] and Euler equations.[11-14] These schemes require large capacities of computer memory to handle the large number of grid points and the associated flow variables. They also require large CPU time to obtain accurate solutions.

For flows with shocks of weak to moderate strength, the potential equation, which assumes irrotational isentropic flows, can satisfactorily be used to solve for these flows, since the entropy increase and vorticity production across the shock are small. The integral equation solution of the potential equation represents an alternative to the finite-difference method (FDM) and finite-volume method (FVM) for treating transonic flows. The integral-equation method (IEM) has several advantages over the finite-difference and finite-volume methods. The IEM involves evaluation of integrals, which is more accurate and simpler than the FDM and FVM, in which the accuracy depends on the grid size since they involve evaluation of derivatives. Moreover, the IEM automatically satisfies the far-field boundary conditions and hence only a small limited region around the source of disturbance is needed. In the FDM and FVM, grid points are needed over a large region around the source of disturbance and special treatment is required to satisfy the far-field boundary conditions.

The computations of the steady transonic flows using integral equation methods started a few years ago. The IE schemes for solving steady transonic flows have been developed based on the TSD equation[15,16] and the full-potential equation.[17-22] For unsteady transonic flows, IE schemes based on the TSD equation have been developed by Nixon,[23] Hounjet,[24] and Tseng and Morino[25] for small-amplitude unsteady motions.

In this paper, we present the unsteady IE scheme based on the full-potential equation formulation. This work is the extension of that of Kandil and Hu.[21,22] The scheme is applied to the unsteady transonic flow of a pitching NACA 0012 airfoil. The results of this scheme are compared with those of an implicit approximate-factorization scheme of the Euler equations of Kandil and Chuang.[13]

Formulation

Full-Potential Equation

For a general unsteady motion of a body, the governing equations are more easily solved if the body-fixed frame of reference formulation is used. In addition to the space-fixed frame of reference $OXYZ$, we introduce the body-fixed frame of reference $oxyz$, which is also known as the moving frame of reference. The moving frame of reference $oxyz$ is translating at a velocity of $V_o(t)$ and rotating around a pivot point r_p at an angular velocity of $\Omega(t)$. Then, we have the following relation:

$$V = V_r + V_o + \Omega \times r \tag{1}$$

where V is the absolute velocity vector, V_r the relative velocity vector, and r the radius vector in the moving frame of reference of the fluid particle measured from pivot point r_p.

After introducing the characteristic parameters of $|V_o|$, the density at infinity ρ_∞ and the length ℓ, the dimensionless form of the full-potential equation in the moving frame of reference is obtained as

$$\nabla^2\Phi = -\frac{\nabla\rho}{\rho}\cdot(\nabla\Phi - e_o - \Omega\times r) - \frac{1}{\rho}\frac{\partial'\rho}{\partial t} \tag{2}$$

with

$$\rho = \left\{1 + \frac{\hat{\gamma}-1}{2}M_\infty^2\left[-\left(\nabla\Phi - e_o - \Omega\times r\right)^2 + \left(e_o + \Omega\times r\right)^2 - 2\left(\frac{\partial'\Phi}{\partial t}\right)\right]\right\}^{\frac{1}{\hat{\gamma}-1}} \tag{3}$$

Received Oct. 15, 1988; revision received July 26, 1989.

*Professor, Department of Mechanical Engineering and Mechanics. Associate Fellow AIAA.

†Research Assistant, Department of Mechanical Engineering and Mechanics; currently Assistant Professor, Hampton University. Member AIAA.

where Φ is the absolute velocity potential given by $V = \nabla\Phi = \nabla'\Phi$, $e_o (= u_o i + v_o j + w_o k)$ the unit vector parallel to V_o, ρ the density, M_∞ the Mach number which is defined as $(V_o^2 \rho_\infty/\hat{\gamma}P_\infty)^{1/2}$, $\hat{\gamma}$ the ratio of specific heats, ρ_∞ and P_∞ the air density and pressure at rest at infinity, respectively, t the time, and the prime refers to the derivative with respect to the moving frame of reference.

For the unsteady two-dimensional flow, as shown in Fig. 1, we have

$$r_p = x_p i \tag{4}$$

$$e_o = u_o i + v_o j \tag{5}$$

$$\Omega = \dot{\alpha} k \tag{6}$$

where

$$\dot{\alpha} = \frac{d\alpha(t)}{dt} \tag{7}$$

Equation (2) thus becomes

$$\Phi_{xx} + \Phi_{yy} = G_1 + G_2 \tag{8}$$

with

$$G_1 = -\frac{1}{\rho}\{(\Phi_x - u_o + \dot{\alpha}y)\rho_x + [\Phi_y - v_o - \dot{\alpha}(x - x_p)]\rho_y\} \tag{9}$$

$$G_2 = -\frac{1}{\rho}\frac{\partial'\rho}{\partial t} \tag{10}$$

where the characteristic length is the airfoil chord length. Similarly, Eq. (3) reduces to

$$\rho = \left[1 + \frac{\hat{\gamma}-1}{2}M_\infty^2\left\{-[\Phi_x - u_o + \dot{\alpha}y]^2 - [\Phi_y - v_o - \dot{\alpha}(x - x_p)]^2 + (u_o - \dot{\alpha}y)^2 + [v_o + \dot{\alpha}(x - x_p)]^2 - 2\left(\frac{\partial'\Phi}{\partial t}\right)\right\}\right]^{\frac{1}{\hat{\gamma}-1}} \tag{11}$$

Equations (8–11) are the basic equations to be solved for two-dimensional unsteady flows in the moving frame of reference.

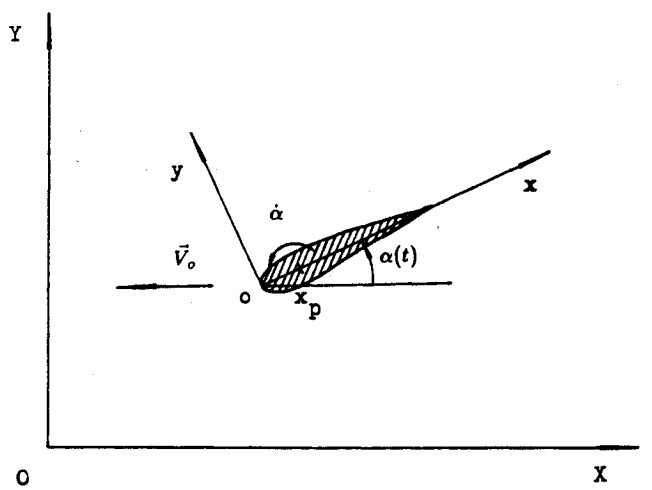

Fig. 1 Physical problem and coordinate system for unsteady flows.

Boundary Conditions

The boundary conditions are given as follows:

1) Surface no-penetration condition:

$$V_r \cdot n_g = 0, \qquad \text{on } g(x, y) = 0 \tag{12}$$

where n_g is the normal unit vector of airfoil surface, $g(x,y) = 0$.

2) Kutta condition:

$$\Delta C_p|_{TE} = 0 \tag{13}$$

This implies that

$$\frac{D}{Dt}\left(\frac{\zeta}{\rho}\right)\bigg|_{TE} = 0 \tag{14}$$

or

$$\frac{\partial'}{\partial t}\left(\frac{\zeta}{\rho}\right)\bigg|_{TE} + V_r \cdot \left(\nabla\frac{\zeta}{\rho}\right)\bigg|_{TE} = 0 \tag{15}$$

where ΔC_p is the pressure jump, ζ the vorticity, and the subscript TE refers to the airfoil trailing edge.

3) Infinity conditions:

$$\nabla\Phi \to 0 \quad \text{away from } g(x, y) = 0 \text{ and } w(x, y, t) = 0 \tag{16}$$

where $w(x, y, t) = 0$ is the wake surface.

4) Wake conditions: The kinematic boundary condition is given by

$$\frac{1}{|\nabla w|}\frac{\partial' w}{\partial t} + V_r \cdot n_w = 0, \qquad \text{on } w = 0 \tag{17}$$

and the dynamic boundary condition is given by

$$\frac{D}{Dt}\left(\frac{\zeta}{\rho}\right) = 0, \qquad \text{on } w = 0 \tag{18}$$

or

$$\frac{\partial'}{\partial t}\left(\frac{\zeta}{\rho}\right) + V_r \cdot \nabla\left(\frac{\zeta}{\rho}\right) = 0 \tag{19}$$

where n_w is the normal unit vector to the wake surface.

Integral Equation Solution

Reading the unsteady full-potential equation (8) as Poisson's equation and using Green's third identity, one can give the integral equation solution of Eq. (8), for the absolute velocity field in the moving frame of reference, as

$$\nabla\Phi(x, y, t) = \frac{1}{2\pi}\oint_g \gamma_g(s, t)\frac{(y-\eta)i - (x-\xi)j}{(x-\xi)^2 + (y-\eta)^2}\,ds + \frac{1}{2\pi}\int\int G_1(\xi, \eta, t)\frac{(x-\xi)i + (y-\eta)j}{(x-\xi)^2 + (y-\eta)^2}\,d\xi d\eta + \frac{1}{2\pi}\int\int G_2(\xi, \eta, t)\frac{(x-\xi)i + (y-\eta)j}{(x-\xi)^2 + (y-\eta)^2}\,d\xi d\eta + \frac{1}{2}\int_w \gamma_w(s, t)\frac{(y-\eta)i - (x-\xi)j}{(x-\xi)^2 + (y-\eta)^2}\,ds \tag{20}$$

where γ_g and γ_w are the airfoil-surface and wake-surface vorticity distributions, respectively. The first integral in Eq. (20) is a surface integral representing the contribution of the airfoil

thickness, camber, and angle of attack; the second and third integrals are field integrals representing the full-compressibility and unsteadiness contributions, respectively; the last integral term is a surface integral representing the wake contribution.

Method of Solution

The steady-state integral-equation with shock-capturing (IE-SC) scheme[17,21,22] has been extended to treat unsteady transonic flows. Because the body-fixed frame of reference is used in the formulation of the problem, the computational domain is fixed in the frame of reference and moves with it. Consideration of the motion of the grid is necessary only if the body is deforming, a case which is not considered in the present paper.

After discretization of the IE solution, Eq. (20) becomes

$$\nabla\Phi(x, y, t) = \frac{1}{2\pi}\sum_{k=1}^{N}\int_{g_k}\gamma_{g,k}(s, t)\frac{(y-\eta)\boldsymbol{i} - (x-\xi)\boldsymbol{j}}{(x-\xi)^2 + (y-\eta)^2}\,\mathrm{d}s + \frac{1}{2\pi}\sum_{i=1}^{IM}\sum_{j=1}^{JM} G_1(t)_{i,j}\int\int_{A_{i,j}}\frac{(x-\xi)\boldsymbol{i} + (y-\eta)\boldsymbol{j}}{(x-\xi)^2 + (y-\eta)^2}\,\mathrm{d}\xi\mathrm{d}\eta + \frac{1}{2\pi}\sum_{i=1}^{IM}\sum_{j=1}^{JM} G_2(t)_{i,j}\int\int_{A_{i,j}}\frac{(x-\xi)\boldsymbol{i} + (y-\eta)\boldsymbol{j}}{(x-\xi)^2 + (y-\eta)^2}\,\mathrm{d}\xi\mathrm{d}\eta + \frac{1}{2\pi}\sum_{k=1}^{M(t)}\gamma(t)_{w,k}\int_{w_k}\frac{(y-\eta)\boldsymbol{i} - (x-\xi)\boldsymbol{j}}{(x-\xi)^2 + (y-\eta)^2}\,\mathrm{d}s \tag{21}$$

where N is the total number of airfoil surface panels, $IM \times JM$ is the total number of the field elements, and $M(t)$ is the total number of the wake point vortices or wake vortex panels, which is a function of time. A surface vortex panel of linear vorticity distribution γ_g and field elements of constant strengths, G_1 and G_2, are used. A wake vortex panel of constant strength γ_w or of the equivalent lumped strength is used.

Unsteady IE-SC Scheme

The unsteady IE-SC scheme is a time-marching iterative scheme, which is outlined as follows: Starting with the initial conditions, which may be a steady flow condition or a condition of rest, one solves Eq. (21) with G_1 and G_2 given by Eqs. (9-11) and with boundary conditions given by Eqs. (12), (13), (17), and (18) iteratively at each time step. It is noted that Eq. (16) is automatically satisfied through the present IE scheme. By the end of the iteration at each time step, we obtain the necessary distribution values: γ_g, γ_w, G_1, and G_2. The wake point vortices or wake vortex panels are generated during each time step and updated at each iteration.

The steps of the unsteady IE-SC time-marching iterative scheme are described as follows:

At Time Step $n = 0$—Steady Flow Initial Conditions

Let the time step $n = 0$ correspond to the steady flow problem and solve the steady flow problem using the steady IE-SC scheme to obtain the initial conditions. The steady IE-SC scheme is given in Ref. 21 by the authors and hence it will not be presented here.

At Time Step n—Unsteady Time-Marching Iterative Scheme

From the previous time steps, $(n-1)$ and $(n-2)$, one has already obtained all necessary distribution values at $(n-1)$ and $(n-2)$ time levels. At the time step (n), the airfoil changes its orientation, and the value of $\dot{\alpha}$ is calculated numerically. One starts the iteration cycle by solving for the necessary distribution values at the (n) time level until the solution converges. The iteration cycle for the time step (n) is given as follows:

Step 1 (enforcing the boundary conditions). In this step, Eq. (21) is used to calculate the absolute velocity at the control points of the airfoil surface. The relative velocity is calculated according to Eq. (1)

$$V_r = \nabla\Phi(x, y, t) - \boldsymbol{e}_o - (\dot{\alpha}\boldsymbol{k}) \times \boldsymbol{r} = (u + \cos\alpha + \dot{\alpha}y)\boldsymbol{i} + [v - \sin\alpha - \dot{\alpha}(x - x_p)]\boldsymbol{j} \tag{22}$$

After one obtains the relative velocity at each control point, Eq. (12) is applied to enforce the no-penetration condition. The solution of Eq. (12) gives the airfoil vortex distribution at time level (n), $\gamma_g^{(n)}$.

Step 2 (wake point vortex generation). The change of the angle of attack in an unsteady motion causes vorticity shedding in the form of a vortex strip along the trailing edge. The vortex strip is convected at the local relative velocity. In the present work, a shed vortex strip is modeled by a lumped point vortex. By using Eqs. (17) and (18), the wake point vortices are generated and thus we obtain $\gamma_{w,k}^{(n)}$ for $k = 1, \ldots, n$. The details of the wake point vortex generation are described in the next subsection.

Step 3 (Computation of $\Phi_t'^{(n)}$). The time-derivative term of velocity potential $\Phi_t'^{(n)}$ could be calculated from $\Phi^{(n)}$ and $\Phi^{(n-1)}$, and hence the potentials $\Phi^{(n)}$ and $\Phi^{(n-1)}$ must be known. They could also be calculated by integrating the velocity field numerically. In order to avoid the numerical error in doing this numerical integration of velocity, Eq. (11) is used to compute the $\Phi_t'^{(n)}$ distributions. Thus, Eq. (11) takes the form

$$\Phi_t'^{(n)} \equiv \left(\frac{\partial'\Phi}{\partial t}\right)^{(n)} = \Phi_t'\left[\Phi_x^{(n-1)}, \Phi_y^{(n-1)}, \rho^{(n-1)}, \alpha^{(n)}, \dot{\alpha}^{(n)}\right] \tag{23}$$

where the Φ_x, Φ_y, and ρ values at time level (n) are replaced by the values at time level $(n-1)$ of the previous iteration, starting from the second iteration.

Step 4 (computation of relative velocity field $V_r^{(n)}$). Equations (21) and (22) are used to compute the relative velocity field. For the first time step $(n = 1)$ at the first iteration, G_2 is set to zero.

Step 5 (computation of $\rho^{(n)}$ and $G_2^{(n)}$). After $\Phi_t'^{(n)}$ in step 3 and $\nabla\Phi^{(n)}$ in step 4 are computed, Eq. (11) is again used to calculate the density distribution which is given by

$$\rho^{(n)} = \rho[\nabla\Phi^{(n)}, \Phi_t^{(n)}, \alpha^{(n)}, \dot{\alpha}^{(n)}] \tag{24}$$

In order to compute $G_2^{(n)}$, one must first calculate the time derivative of density $\rho_t'^{(n)}$. The value of $\rho_t'^{(n)}$ is calculated numerically by using second-order-accurate backward differencing. Then, Eq. (10) is used to calculate $G_2^{(n)}$.

Step 6 (computation of $M^{(n)}$, $\rho_x^{(n)}$, $\rho_y^{(n)}$, and $G_1^{(n)}$). The local Mach number is computed from the equation

$$M^{(n)}(x, y, t) = \frac{M_\infty|V_r^{(n)}(x, y, t)|}{[\rho^{(n)}(x, y, t)]^{\frac{\hat{\gamma}-1}{2}}} \tag{25}$$

Based on the computed local Mach numbers, the Murman-Cole type differencing is used to calculate the spatial derivatives of $\rho_x^{(n)}$ and $\rho_y^{(n)}$. Then Eq. (9) is used to calculate $G_1^{(n)}$.

Step 7 (computation of surface pressure coefficients $C_p^{(n)}$). The surface pressure coefficient $C_p^{(n)}$ is calculated by

$$C_p = \frac{2}{\hat{\gamma}M_\infty^2}(\rho^{\hat{\gamma}} - 1) \tag{26}$$

Step 8 (convergence criterion). If $C_p^{(n)}$ converges at every surface control point, then we go to time step $(n+1)$; otherwise, steps 1-8 are repeated to update all quantities at time level (n).

At Time Step $(n+1)$

The airfoil changes its orientation to another position and steps 1-8 are repeated for time step $(n+1)$.

Wake Point Vortex Generation

As previously mentioned, the change of the angle of attack during the unsteady pitching motion causes vorticity shedding from the trailing edge. The generation of the wake point vortexes has been discussed in step 2 above. Now, more details on the generation are given below.

At Time Step n = 0

This time step corresponds to steady flow, and hence there is no wake vorticity shedding from the airfoil trailing edge.

At Time Step n = 1

When the airfoil changes angle of attack from $\alpha^{(0)}$ to $\alpha^{(1)}$, a strip of vorticity is shed from the trailing edge. The shed vorticity is modeled by a point vortex which is placed at the middle point of this strip. The direction of this vortex strip is determined by Eq. (17) or by the fact that the local relative velocity is tangential to the vortex strip. The length of the strip $\Delta_{s_{w,1}}$ is determined by

$$\Delta s_{w,1}^{(n)} = |V_r|_{\text{TE}}^{(n)} (\Delta t)^{(n)} \tag{27}$$

where $|V_r|_{\text{TE}}^{(n)}$ is the magnitude of the relative velocity at trailing edge and the second subscript "1" refers to the first point vortex. Equation (22) is used to calculate the relative velocity at the trailing edge. The strength of the wake point vortex is determined by Eq. (18), or equivalently by

$$\left(\frac{\Gamma}{\rho}\right)_{w,1}^{(n)} = \left[\Sigma_g \left(\frac{\Gamma}{\rho}\right)_g\right]^{(n-1)} - \left[\Sigma_g \left(\frac{\Gamma}{\rho}\right)_g\right]^{(n)} \tag{28}$$

where the summation is taken over the airfoil surface and Γ is the circulation around the airfoil surface panel ($\Gamma \equiv \int_{\text{panel}} \gamma \, dl$) or the circulation of the wake point vortex. The location and the circulation of this point vortex is updated during this time step and at each iteration.

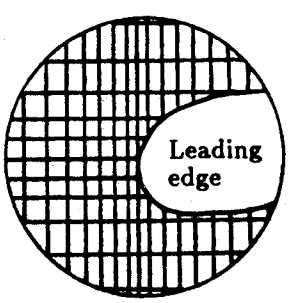

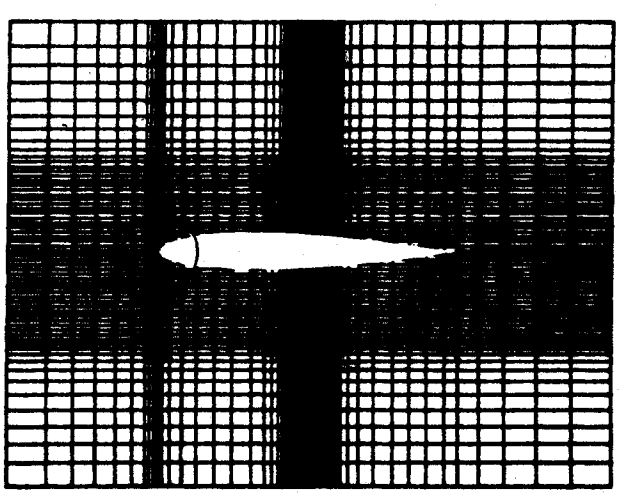

Fig. 2 Typical rectangular grid.

At Time Step n = 2

When the airfoil changes angle of attack from $\alpha^{(1)}$ to $\alpha^{(2)}$, a new point vortex is shed from the trailing edge while the old point vortex shed during the previous time step is now convected downstream with the local relative velocity. The location and the strength of the newly shed point vortex are determined in the same way as that of the time step $n = 1$.

At Time Step n = 3, 4 ...

In general, at each time step, a new wake point vortex is shed from trailing edge. At the same time, all of the old point vortexes are convected downstream with the relative velocity.

It should be noted that the generation of the wake vortex is one of the most important parts of the unsteady integral equation method.

Computational Example

The unsteady IE-SC scheme has been applied to the NACA 0012 airfoil at a freestream Mach number of 0.755 undergoing

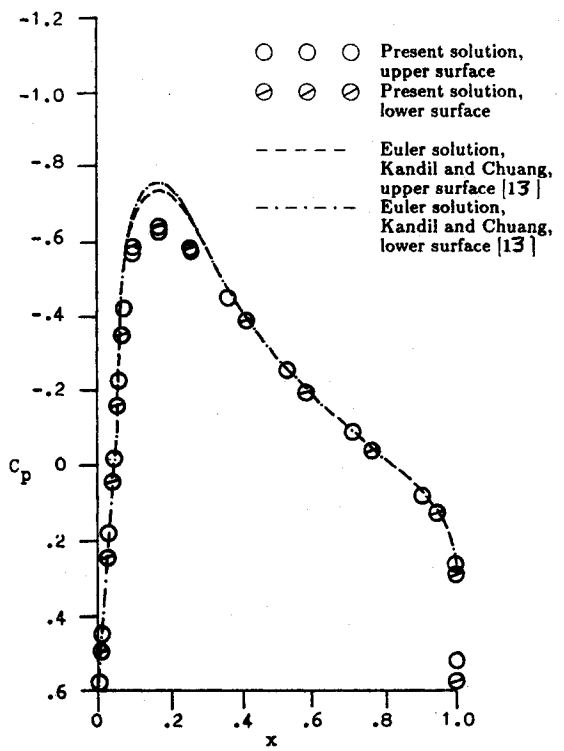

Fig. 3 Initial condition of C_p.

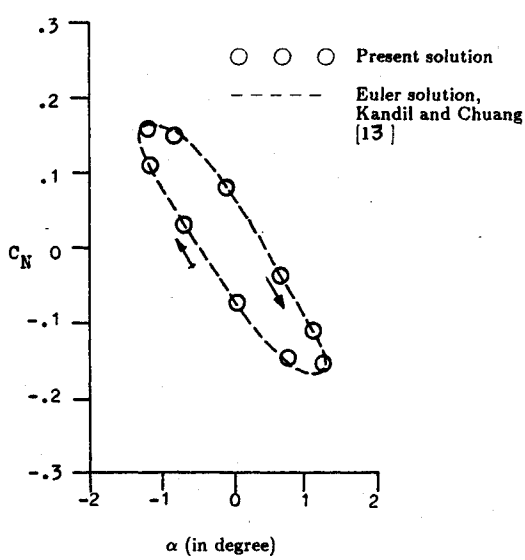

Fig. 4 Normal-force coefficient.

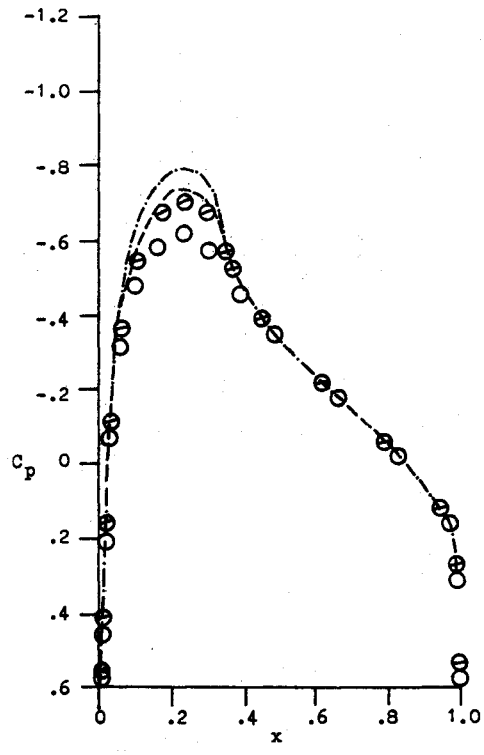

a) $\alpha(t) = 0.729°$, $k_c t = 35°$

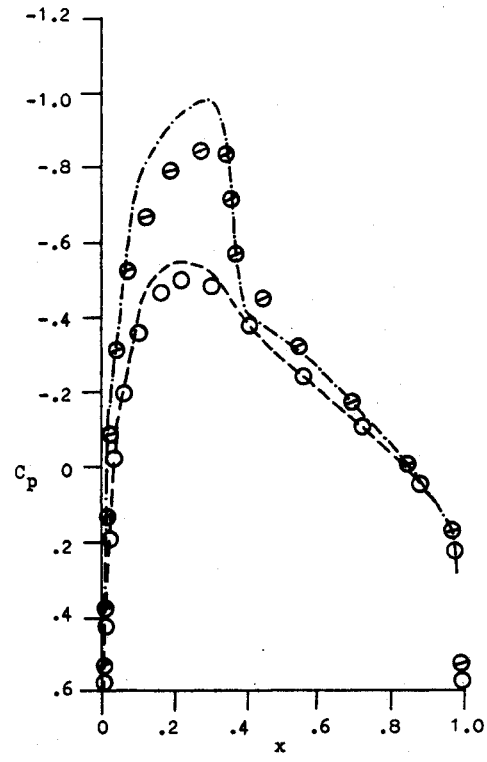

c) $\alpha(t) = 1.235°$, $k_c t = 104°$

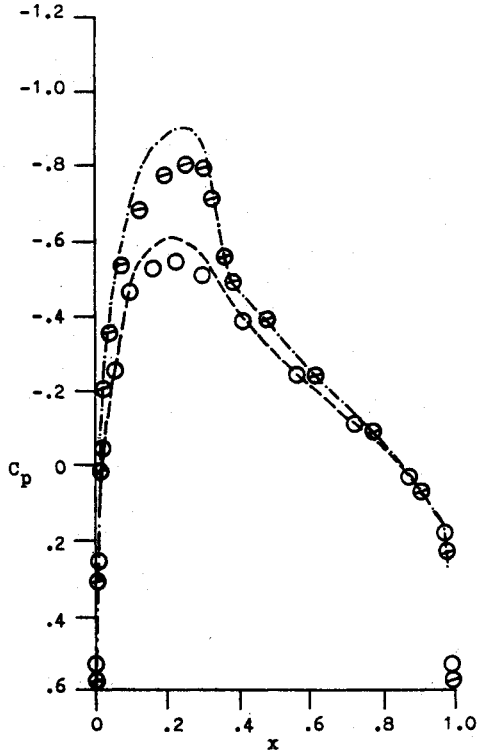

b) $\alpha(t) = 1.189°$, $k_c t = 70°$

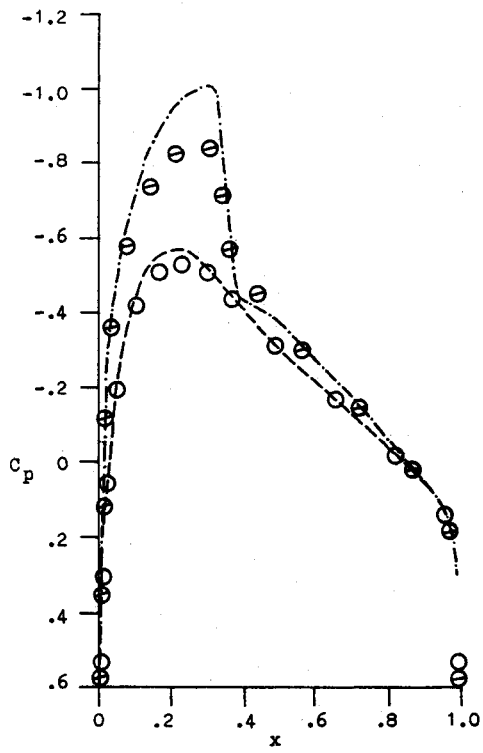

d) $\alpha(t) = 0.848°$, $k_c t = 139°$

Fig. 5 Time history of C_p (◯: present solution, upper surface; ⊘: present solution, lower surface; — — —: Euler solution, upper surface[13]; — · — · —: Euler solution, lower surface[13]). (continued)

a forced pitching oscillation around a pivot point at the quarter-chord length measured from the leading edge ($x_p = 0.25$). The angle of attack $\alpha(t)$ is given by

$$\alpha(t) = \alpha_0 + \alpha_a \sin(k_c t) \tag{29}$$

where $\alpha_0 = 0.016$ deg, $\alpha_a = 1.255$ deg, and $k_c = 0.1632$, and where k_c is the reduced frequency based on the chord length.

Figures 2–4 show the present computed results and the finite-volume Euler solution produced by Kandil and Chuang[13] who used the implicit approximately factored Euler solver in a moving frame of reference.

The computational domain used in this unsteady flow case is 2×1.5 chord lengths with 64×60 field elements. Rectangular elements are used everywhere except at the airfoil surface where trapezoidal elements are used; see Fig. 2. A total of 102

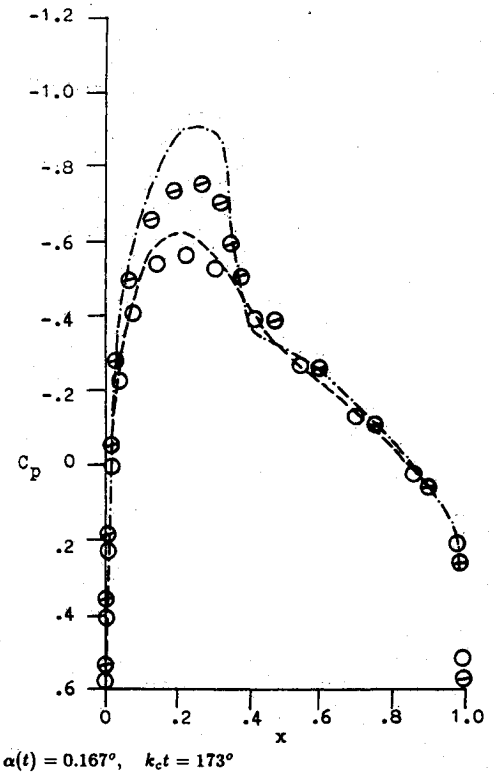

e) $\alpha(t) = 0.167°$, $k_c t = 173°$

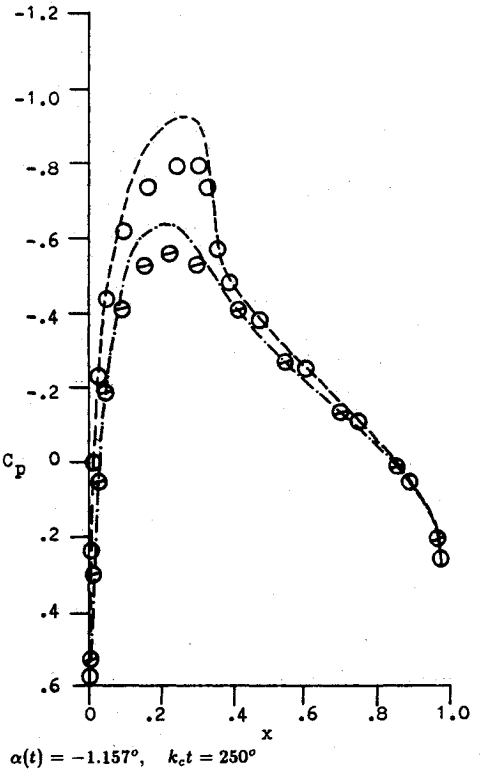

g) $\alpha(t) = -1.157°$, $k_c t = 250°$

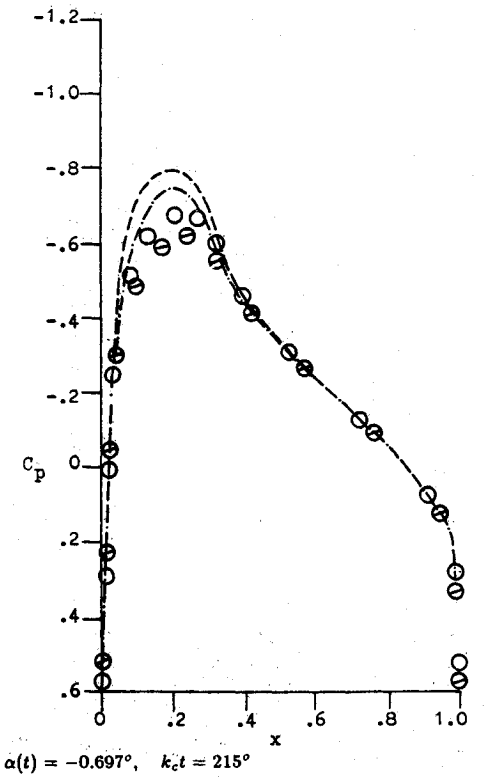

f) $\alpha(t) = -0.697°$, $k_c t = 215°$

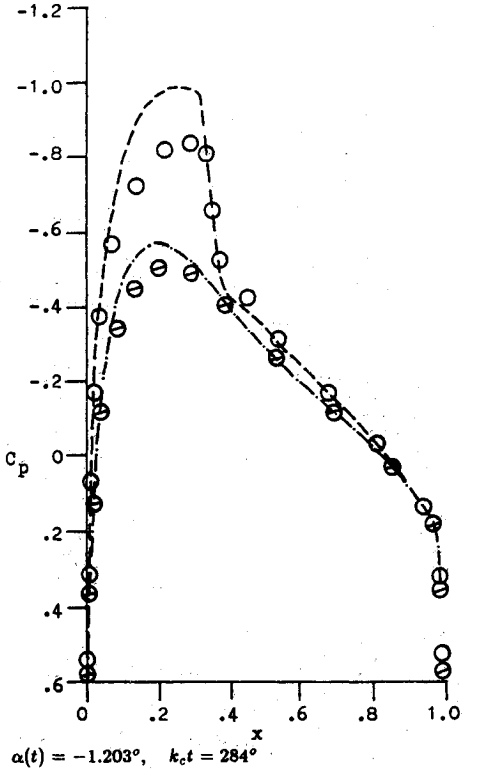

h) $\alpha(t) = -1.203°$, $k_c t = 284°$

Fig. 5 (continued) Time history of C_p (◯: present solution, upper surface; ⊘: present solution, lower surface; — — —: Euler solution, upper surface[13]; — · — · —: Euler solution, lower surface[13]). (continued)

uniform times steps is needed for one cycle of oscillation, and 10 iterations per time step are needed to achieve convergence for one time step. The periodic solution is obtained after two cycles of oscillation.

The initial condition corresponds to the steady flow solution at the mean angle of attack of $\alpha_0 = 0.016$ deg with $M_\infty = 0.755$. The computed steady solution is shown in Fig. 3 along with the Euler-equation solution.[13] The comparison shows that the steady peak pressure predicted by the present unsteady IE-SC scheme is lower than that of the Euler solution. This is typical of the results of the present IE-SC scheme and the Euler scheme, as has been shown in the previous steady computations.[21,22] The peak pressure predicted by the IE scheme is slightly lower than that of experimental data, and the peak pressure predicted by the Euler solution is usually higher than that of the experimental data.

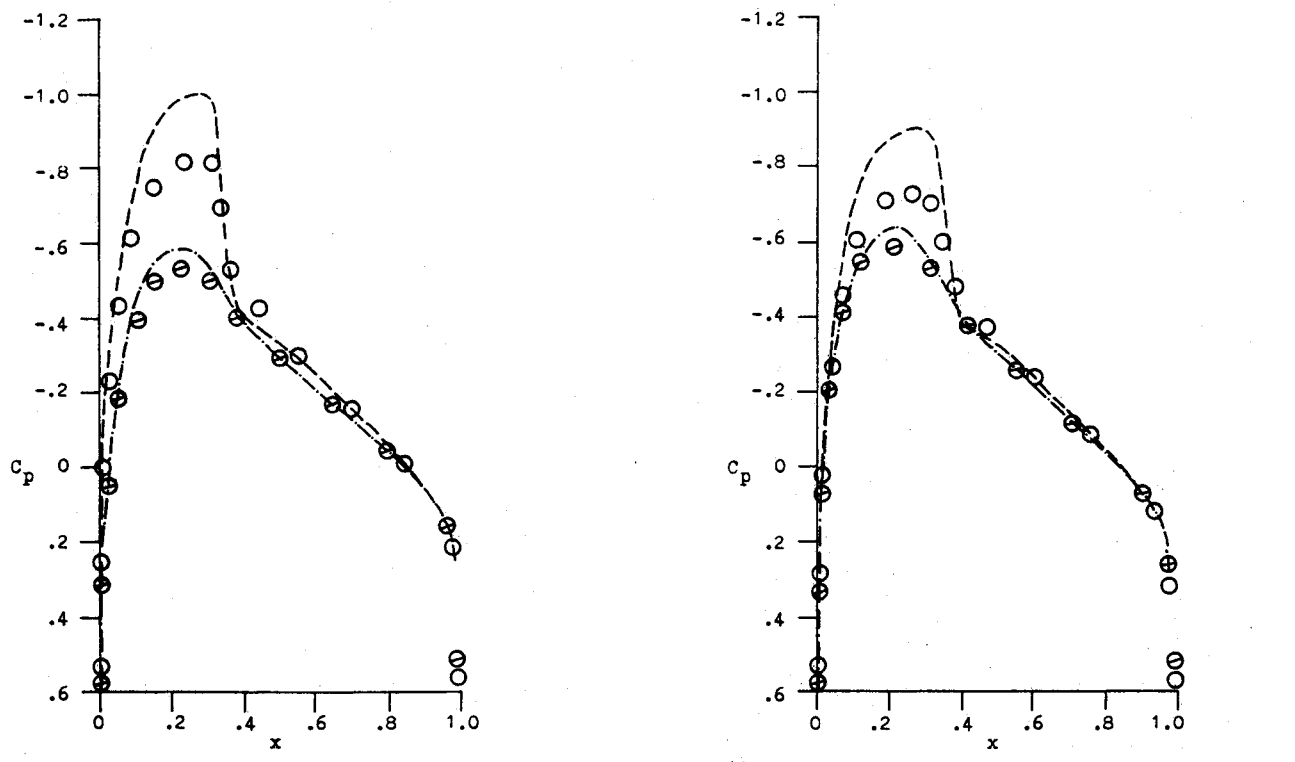

i) $\alpha(t) = -0.816°$, $k_c t = 319°$ j) $\alpha(t) = -0.135°$, $k_c t = 354°$

Fig. 5 (continued) Time history of C_p (◯: present solution, upper surface; ⊘: present solution, lower surface; — — —: Euler solution, upper surface[13]; — · — · —: Euler solution, lower surface[13]).

Figure 4 shows the computed periodic normal-force coefficient C_N for this pitching motion case. It should be noted here that the positive and negative angles of attack correspond to clockwise and counterclockwise rotations, respectively, according to Fig. 1. The normal-force coefficient C_N is calculated by

$$C_N = \int_0^1 (C_{pl} - C_{pu})\, dx \tag{30}$$

The comparison with the Euler solution[13] shows good agreement. Figure 5 shows the corresponding periodic instantaneous surface pressure coefficients for one cycle of the motion and the Euler solution.[13] The comparison shows that the unsteady pressure history is consistent with that of the Euler solution,[13] except that the upper and lower surface peak pressure coefficients are lower than those of the Euler solution. This difference has already existed in the steady initial condition as shown in Fig. 3. The unsteady motion of the shock, which includes the change of the shock strength, the generation and loss of the shock, and the change of the shock location, is in a good agreement with the Euler solution,[13] with the exception that the shock strength is smaller than that of the Euler solution.

Concluding Remarks

The full-potential equation formulation in a moving frame of reference has been used to solve for unsteady transonic flows. The unsteady IE-SC scheme has been developed. The resulting unsteady IE-SC scheme has been applied to a NACA 0012 airfoil undergoing a pitching oscillation. The numerical results are compared with the results of an implicit, approximately factored, finite-volume Euler scheme. Although the motion of the shock has been correctly predicted, the predicted surface pressure has peaks lower than those predicted by the Euler solver. However, it is also recalled that the Euler solution overpredicts experimental pressure peaks.

The unsteady IE-SC scheme is efficient in terms of the number of iterations as compared to the other existing schemes, which use finite-difference or finite-volume methods throughout large computational domains with fine grids. If the influence coefficients of the field elements are stored in the core memory of the computer, the computational time can be substantially reduced since the field-element calculations take about 80% of the computational time per iteration. It is recommended that the integral equation with shock capturing-shock fitting (IE-SCSF) and integral equation with embedded Euler domain (IE-EE) schemes[21,22] for steady flow be extended to unsteady transonic flow problems.

Acknowledgment

This research work is supported by NASA Langley Research Center under Grant NAG 1-648.

References

[1]Ballhaus, W. F. and Lomax, H., "Numerical Solution of Low-Frequency Unsteady Transonic Flowfields," *Lecture Notes in Physics*, Vol. 35, Jan. 1975, p. 57–63

[2]Ballhaus, W. F. and Steger, J. L., "Implicit-Approximate-Factorization Scheme for the Low-Frequency Transonic Equation," NASA TM X-73082, 1975.

[3]Ballhaus, W. F. and Goorjian, P. M., "Implicit Finite-Difference Computations of Unsteady Transonic Flows about Airfoil," *AIAA Journal*, Vol. 15, No. 12, Dec. 1977, pp. 1728–1735.

[4]Rizzetta, D. P. and Chin, W. C., "Effects of Frequency in Unsteady Transonic Flow," *AIAA Journal*, Vol. 17, July 1979, pp. 779–781.

[5]Whitlow, W., Jr., "XTRAN2L: A Program for Solving the General Frequency Unsteady Transonic Small Disturbance Equation," NASA TM-85723, Nov. 1983.

[6]Edwards, J. W., Bland, S. R., and Seidel, D. A., "Experience with Transonic Unsteady Aerodynamic Calculations," AGARD CP-374, 1985.

[7]Goorjian, P. M. and Guruswamy, G. P., "Unsteady Transonic Aerodynamic and Aeroelastic Calculations about Airfoils and Wings," AGARD CP-374, 1985.

[8]Isogai, K., "Calculation of Unsteady Transonic Flow Using the Full-Potential Equation," AIAA Paper 77-448, Jan. 1977.

[9]Chapman, R. and Jameson, "Fully Conservative Numerical Solutions for Unsteady Irrotational Transonic Flow about Airfoils," AIAA Paper 79-1555, July 1979.

[10]Goorjian, P. M., "Implicit Computation of Unsteady Transonic Flow Governed by the Full-Potential Equation in Conservative Form," AIAA Paper 80-150, Jan. 1980.

[11]Magnus, R. and Yoshihara, H., "The Transonic Oscillating Flap," AIAA Paper 76-327, Jan. 1976.

[12]Chyu, W. J., Davis, S. S., and Chang, K. S., "Calculating of Unsteady Transonic Flows over an Airfoil," AIAA Paper 79-1554r, July 1979.

[13]Kandil, O. A., and Chuang, H. A., "Unsteady Vortex-Dominated Flows around Maneuvering Wings over a Wide Range of Mach Numbers," AIAA Paper 88-0317, Jan. 1988.

[14]Anderson, W., Thomas, J., and Ramsey, C., "Extension and Applications of Flux-Vector Splitting to Unsteady Calculations on Dynamic Meshes," AIAA Paper 87-1152-CP, July 1987.

[15]Piers, W. J. and Sloff, J. W., "Calculations of Transonic Flow by Means of a Shock-Capturing Field Panel Method," AIAA Paper 79-1459, July 1979.

[16]Ogana, W., "Boundary-Element Methods in Two-Dimensional Transonic Flows," *Boundary Elements IX, Vol. 3: Fluid Flow and Potential Applications,* edited by C. A. Brebbia, W. L. Wendland, and G. Kuhu, Computational Mechanics Publications, Springer-Verlag, London, 1987, pp. 567–582.

[17]Kandil, O. A. and Yates, E. C., Jr., "Computation of Transonic Vortex Flow Past Delta Wings – Integral Equation Approach," *AIAA Journal*, Vol. 24, Nov. 1986, pp. 1729–1236.

[18]Oskam, B., "Transonic Panel Method for the Full-Potential Equation Applied to Multicomponent Airfoils," *AIAA Journal,* Vol. 23, Sept. 1985, pp. 1327–1334.

[19]Erickson, L. L. and Strande, S. M., "A Theoretical Basis for Extending Surface-Paneling Methods to Transonic Flow," *AIAA Journal,* Vol. 23, Dec. 1985, pp. 1860–1867.

[20]Sinclair, P. M., "An Exact Integral (Field Panel) Method for the Calculation of Two-Dimensional Transonic Potential Flow around Complex Configurations," *Aeronautical Journal*, Vol. 90, No. 896, June/July 1986, pp. 227–236.

[21]Kandil, O. A. and Hu, H., "Full-Potential Integral Solution for Transonic Flows with and without Embedded Euler Domains," AIAA Paper 87-1461, 1987; also *AIAA Journal*, Vol. 26, Sept. 1988, pp. 1079–1086.

[22]Kandil, O. A. and Hu, H., "Transonic Airfoil Computation Using the Integral Equation with and without Embedded Euler Domains," *Boundary Elements IX, Vol. 3: Fluid Flow and Potential Applications,* edited by C. A. Brebbia, W. L. Wendland, and G. Kuhn, Computational Mechanics Publications, Springer-Verlag, London, 1987, pp. 553–566.

[23]Nixon, D., "Calculation of Unsteady Transonic Flows Using the Integral Equation Method," *AIAA Journal*, Vol. 16, Sept. 1976, pp. 976–983.

[24]Hounjet, M. H. L., "Transonic Panel Method to Determine Loads on Oscillating Airfoils with Shocks," *AIAA Journal,* Vol. 19, May 1979, pp. 559–566.

[25]Tseng, K. and Morino, L., "Nonlinear Green's Function Methods for Unsteady Transonic Flows," *Transonic Aerodynamics*, edited by D. Nixon, AIAA, New York, 1981, pp. 565–603.